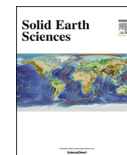


Available online at www.sciencedirect.com

ScienceDirect

Solid Earth Sciences 1 (2016) 89–100

www.elsevier.com/locate/SESCI

Non-monotonic compositional dependence of isothermal bulk modulus of the $(\text{Mg}_{1-x}\text{Mn}_x)\text{Cr}_2\text{O}_4$ spinel solid solutions, and its origin and implication

Xi Liu^{a,b,*}, Zhihua Xiong^{a,b}, Sean R. Shieh^c, Qiang He^{a,b,d}, Liwei Deng^{a,b,e}, Yanyao Zhang^{a,b},
Linlin Chang^{a,b}, Fei Wang^{a,b}, Xinguo Hong^f, Zhiqiang Chen^g^a Key Laboratory of Orogenic Belts and Crustal Evolution, Ministry of Education of China, Beijing 100871, China^b School of Earth and Space Sciences, Peking University, Beijing 100871, China^c Department of Earth Sciences, University of Western Ontario, London, Ontario N6A 5B7, Canada^d Institute of Fluid Physics, China Academy of Engineering Physics, Mianyang 659000, China^e Key Laboratory of Earth and Planetary Physics, Institute of Geology and Geophysics, Chinese Academy of Sciences, Beijing 100029, China^f Mineral Physics Institute, State University of New York, Stony Brook, NY 11974, USA^g Center for High Pressure Science and Technology Advanced Research, 1690 Cailun Road, Pudong, Shanghai 201203, China

Received 24 May 2016; revised 9 July 2016; accepted 16 August 2016

Available online 3 September 2016

Abstract

The compressibility of the spinel solid solutions, $(\text{Mg}_{1-x}\text{Mn}_x)\text{Cr}_2\text{O}_4$ with $x = 0.00$ (0), 0.20 (0), 0.44 (2), 0.61 (2), 0.77 (2) and 1.00 (0), has been investigated by using a diamond-anvil cell coupled with synchrotron X-ray radiation up to ~ 10 GPa (ambient T). The second-order Birch–Murnaghan equation of state was used to fit the P – V data, yielding the following values for the isothermal bulk moduli (K_T), 198.2 (36), 187.8 (87), 176.1 (32), 168.7 (52), 192.9 (61) and 199.2 (61) GPa, for the spinel solid solutions with $x = 0.00$ (0), 0.20 (0), 0.44 (2), 0.61 (2), 0.77 (2) and 1.00 (0), respectively (K_T' fixed as 4). The K_T value of the MgCr_2O_4 spinel is in good agreement with existing experimental determinations and theoretical calculations. The correlation between the K_T and x is not monotonic, with the K_T values similar at both ends of the binary MgCr_2O_4 – MnCr_2O_4 , but decreasing towards the middle. This non-monotonic correlation can be described by two equations, $K_T = -49.2(11)x + 198.0(4)$ ($x \leq \sim 0.6$) and $K_T = 92(41)x + 115(30)$ ($x \geq \sim 0.6$), and can be explained by the evolution of the average bond lengths of the tetrahedra and octahedra of the spinel solid solutions. Additionally, the relationship between the thermal expansion coefficient and composition is correspondingly reinterpreted, the continuous deformation of the oxygen array is demonstrated, and the evolution of the component polyhedra is discussed for this series of spinel solid solutions. Our results suggest that the correlation between the K_T and composition of a solid solution series may be complicated, and great care should be paid while estimating the K_T of some intermediate compositions from the K_T of the end-members.

Copyright © 2016, Guangzhou Institute of Geochemistry. Production and hosting by Elsevier B.V. This is an open access article under the CC BY-NC-ND license (<http://creativecommons.org/licenses/by-nc-nd/4.0/>).

Keywords: Bulk modulus; Non-monotonic correlation; Spinel solid solutions $(\text{Mg}_{1-x}\text{Mn}_x)\text{Cr}_2\text{O}_4$; Synchrotron X-ray radiation

1. Introduction

Isothermal bulk modulus (K_T) is an important parameter in studies of the deep interior of the Earth (e.g., Duffy and Wang,

1998). It has been intensively investigated by different techniques such as high- P compression experiment (e.g., Mao et al., 1969; Hazen, 1993; Fei and Mao, 1993; Shieh et al., 2006), ultrasonic interferometry (e.g., Liebermann et al., 1977; Li et al., 1998), Brillouin scattering (e.g., Weidner et al., 1984; Jackson et al., 2000), empirical calculation (e.g., Anderson and Nafe, 1965; Hazen and Yang, 1999), advanced theoretical simulation (Oganov et al., 2000; Deng et al., 2010), and many more. In the last century, much

* Corresponding author. School of Earth and Space Sciences, Peking University, Beijing 100871, China. Fax: +86 10 6275 2996.

E-mail address: xi.liu@pku.edu.cn (X. Liu).

Peer review under responsibility of Guangzhou Institute of Geochemistry.

knowledge about the K_T of minerals has been obtained and enormously expanded our understanding about the geochemical and geophysical process of the deep Earth (e.g., Ricolleau et al., 2009; Liu et al., 2012).

With some notable exceptions (e.g., Mao et al., 1969; Hazen, 1993; Higo et al., 2006; Liu et al., 2011; Nestola et al., 2011a; He et al., 2012; Yamanaka et al., 2013; Huang and Chen, 2014; Du et al., 2015), numerous experimental investigations have been devoted to determining the K_T of pure end-members of minerals. Most geologically important minerals like olivine (Ol), pyroxene, garnet (Grt), spinel (“spinel” *sensu lato*; Sp), plagioclase, amphibole and mica, however, are extremely complicated solid solutions, in terms of mineral chemistry and crystal structure. Consequently, the K_T values of a series of solid solutions may vary significantly (He et al., 2012). And more importantly, they may have a complicated compositional dependence, as recently demonstrated by Du et al. (2015) for the pyrope-grossular Grt solid solutions ($(\text{Mg}_{1-x}\text{Ca}_x)_3\text{Al}_2\text{Si}_3\text{O}_{12}\text{-Grt}_{\text{ss}}$). On the other hand, large amounts of direct experimental determinations on the K_T values of different compositions for one series of solid solutions are usually unavailable, and the potentially complicated compositional effect is often unquantified. As a result, the K_T values for the minerals with compositions practically relevant to the Earth have to be approximated from the measurements on the end-members by assuming a generally linear compositional dependence (e.g., Powell and Holland, 1985; Ita and Stixrude, 1992; Stixrude and Lithgow-Bertelloni, 2005). Alternatively, they may be simply assumed as compositionally independent (e.g., Cammarano et al., 2005a, 2005b). This is hardly satisfactory. When the mineral solid solutions vary their compositions, the lengths and characteristics of their chemical bonds, and the relative sizes and roles of their component polyhedra may vary significantly and in complicated ways, so that their K_T values can not be easily predicted, as demonstrated here for the Sp solid solution series (Sp_{ss}) along the $\text{MgCr}_2\text{O}_4\text{-Sp}$ and $\text{MnCr}_2\text{O}_4\text{-Sp}$ join in this study.

Chromium spinels have the general chemical formula MCr_2O_4 and the space group $Fd\bar{3}m$ (No. 227; $Z = 8$). In their structure, the oxygens form a cubic close packing array (equipoint $32e$), the M cations occupy one eighth of the tetrahedral (equipoint $8a$) sites and the Cr^{3+} cations occupy half of the octahedral (equipoint $16d$) sites. Due to the large excess octahedral crystal field stabilization energy of Cr^{3+} (-160 kJ/mol; O'Neill and Navrotsky, 1984), significant disordering (cations M and Cr^{3+} switching their sites) is not expected. This gives us an opportunity to closely examine the influence of the compositional variation of the tetrahedral sites on the bond lengths of different chemical bonds, the volumetric systematics of different component polyhedra, and the K_T values of the $\text{MCr}_2\text{O}_4\text{-Sp}$. The result may deepen our understanding of the controlling factors of the K_T of other mineral solid solutions.

$\text{MgCr}_2\text{O}_4\text{-Sp}$ plays a very important role in the partial melting process of the upper mantle (Liu and O'Neill, 2004). With the substitution of Mg by Mn on the tetrahedral sites, a large range of solid solutions may form, as implied by some

field work conducted a long time ago (Graham, 1978; Paraskevopoulos and Economou, 1981). Recently we synthesized a full series of Sp solid solutions along the join $\text{MgCr}_2\text{O}_4\text{-MnCr}_2\text{O}_4$, abbreviated as $(\text{Mg}_{1-x}\text{Mn}_x)\text{Cr}_2\text{O}_4\text{-Sp}_{\text{ss}}$ hereafter, and directly confirmed those field observations (Wang et al., 2012). Considering the large size difference ($\sim 12\%$) between the Mg^{2+} (0.585 Å) and Mn^{2+} (0.655 Å) on a tetrahedral site (O'Neill and Navrotsky, 1983), this is important. Additionally, we investigated the volume-composition relationship, and determined the effect of the Mg–Mn substitution on the thermal expansivities (Wang et al., 2012).

In this study, we conducted a large number of high- P experiments to investigate the compressibility of the $(\text{Mg}_{1-x}\text{Mn}_x)\text{Cr}_2\text{O}_4\text{-Sp}_{\text{ss}}$, and found a non-monotonic compositional effect on the K_T . On the basis of the new result, we reexamined the compositional effect on the thermal expansion coefficients reported by Wang et al. (2012), and discovered a non-monotonic compositional effect as well. Furthermore, we explored the origin of this non-monotonic compositional effect by resorting to the variations of the constituent chemical bonds, the distortion evolution of the oxygen array and the mixing behaviors of the component polyhedra in the $(\text{Mg}_{1-x}\text{Mn}_x)\text{Cr}_2\text{O}_4\text{-Sp}_{\text{ss}}$, and discussed some of its implications to other mineral solid solutions pertinent to the geosciences.

2. Experiments

The $(\text{Mg}_{1-x}\text{Mn}_x)\text{Cr}_2\text{O}_4\text{-Sp}_{\text{ss}}$, with $x = 0.00$ (0), 0.20 (0), 0.44 (2), 0.61 (2), 0.77 (2) and 1.00 (0), were synthesized in an open air at 1200 °C for 48 h by using a conventional muffle furnace (Wang et al., 2012). Their compositional and powder X-ray diffraction (XRD) data suggested that they were essentially 2–3 spinels, with nearly all Mg^{2+} cations and Mn cations (appearing as Mn^{2+}) on the tetrahedral sites and nearly all Cr cations (occurring as Cr^{3+}) on the octahedral sites. This observation was fully compatible with previous studies (Raccach et al., 1966; O'Neill and Dollase, 1994; Gilewicz-Wolter et al., 2005; Stefan and Irvine, 2011). Arguably, a trace amount of Cr^{4+} or Cr vacancy might be present according to O'Neill and Dollase (1994) or Moriwake et al. (2002), respectively, but its amount is too small to be meaningful to the physical properties of the Sp_{ss} .

To investigate the compression behavior, we have carried out high- P powder X-ray diffraction experiments (ambient T) at the beamline X17C, National Synchrotron Light Source, Brookhaven National Laboratory. We compressed the $(\text{Mg}_{1-x}\text{Mn}_x)\text{Cr}_2\text{O}_4\text{-Sp}_{\text{ss}}$ up to ~ 10 GPa with a symmetrical diamond-anvil cell (DAC). Since the experimental techniques have been well established and routinely used by our group (e.g., Liu et al., 2009, 2011; Chang et al., 2013; Xiong et al., 2015), they are only briefly described here. We used T301 stainless steel plates as the gaskets, a 1:4 ethanol-methanol mixture as the pressure media, and the ruby fluorescence method as the P scale (Mao et al., 1978). The incident synchrotron X-ray beam was monochromatized to a wavelength of either 0.4066 or 0.4112 Å, and its beam size was collimated

to a size of about $\sim 25 \times 20 \mu\text{m}^2$. The X-ray diffraction data were collected for 600–1200 s using an online CCD detector, and later processed to generate the conventional one-dimension X-ray profile using the Fit2D program (Hammersley, 1996). With a full profile refinement of the collected X-ray data, the positions of the diffraction peaks such as 111, 220, 311, 222, 400, 331, 422, 511, 440 and 531 were determined, and the unit-cell parameters of the $(\text{Mg}_{1-x}\text{Mn}_x)\text{Cr}_2\text{O}_4\text{-Sp}_{\text{ss}}$ at different P were subsequently refined from them.

3. Results and discussions

Our high- P experiments for the $\text{MgCr}_2\text{O}_4\text{-Sp}$ were conducted up to ~ 10.3 GPa. According to Wang et al. (2002), Yong et al. (2012) and Nestola et al. (2014), no phase transition should be expected for this Sp_{ss} in the investigated P range, which was confirmed by the present DAC experiments. Furthermore, the high- P experiments for other $(\text{Mg}_{1-x}\text{Mn}_x)\text{Cr}_2\text{O}_4\text{-Sp}_{\text{ss}}$ with $x = 0.20$ (0), 0.44 (2), 0.61 (2), 0.77 (2) and 1.00 (0) were carried out up to ~ 5.46 , 10.33, 5.84, 7.56 and 9.12 GPa, respectively. No phase transition was observed in these compression experiments as well. Table 1 summarises the unit-cell parameters at different pressures derived from our X-ray diffraction patterns. In total, 42 sets of unit-cell parameters have been obtained for the $(\text{Mg}_{1-x}\text{Mn}_x)\text{Cr}_2\text{O}_4\text{-Sp}_{\text{ss}}$ in this study.

3.1. K_T of the $\text{MgCr}_2\text{O}_4\text{-Sp}$

Fig. 1 shows the P – V data of the $\text{MgCr}_2\text{O}_4\text{-Sp}$ obtained in this study, along with the P – V data from previous experimental investigations (up to 19.49 GPa by Yong et al. (2012) and up to 9.2 GPa by Nestola et al. (2014)). All data at P below ~ 14 GPa from these different studies appear in good agreement. Due to the somehow imperfect performance of the employed pressure medium of argon in maintaining a hydrostatic condition in the DAC experiments at high P (Klotz et al., 2009), the two data at ~ 14 GPa reported by Yong et al. (2012) might be subject to minor P overestimate only, but the two data at 18 and 19.49 GPa should have been significantly affected (Fig. 1). Anyhow, these four data are not particularly meaningful since the maximum stable P for the $\text{MgCr}_2\text{O}_4\text{-Sp}$ at geologically relevant T is less than ~ 14 GPa (Ishii et al., 2015).

The reduction of the unit-cell volume of the $\text{MgCr}_2\text{O}_4\text{-Sp}$ achieved by our DAC experiments was $\sim 4.64\%$ only (Table 1). Considering this relatively small volume reduction, we have chosen to fit the P – V data to the second-order Birch–Murnaghan EoS (BM-EoS; Birch, 1947) by a least-squares method, in order to determine the K_T :

$$P = 3K_T f_E (1 + 2f_E)^{\frac{5}{2}}, \quad (1)$$

where f_E is the Eulerian definition of finite strain, $[(V_0/V)^{2/3} - 1]/2$. In the Eulerian definition of the finite strain, V_0 and V are the volume at zero pressure and high pressure, respectively. The first derivative of K_T , K'_T , is thus assumed as 4.

Table 1
Unit-cell parameters of $(\text{Mg}_{1-x}\text{Mn}_x)\text{Cr}_2\text{O}_4\text{-Sp}_{\text{ss}}$ at different pressures (ambient T)^a.

x	P (GPa) ^b	a (Å)	V (Å ³)	
0.00 (0) ^c	0.0001 (0)	8.3364 (1)	579.34 (1)	
	0.50 (5)	8.3237 (6)	576.69 (12)	
	1.81 (5)	8.3069 (11)	573.22 (22)	
	3.24 (5)	8.2884 (7)	569.38 (14)	
	4.30 (5)	8.2740 (10)	566.42 (19)	
	6.23 (5)	8.2505 (4)	561.61 (8)	
	7.31 (5)	8.2436 (16)	560.21 (33)	
	8.39 (5)	8.2296 (9)	557.36 (18)	
	9.28 (5)	8.2219 (3)	555.80 (7)	
	10.32 (5)	8.2071 (10)	552.80 (21)	
	0.20 (0)	0.0001 (0)	8.3579 (1)	583.83 (1)
0.74 (10)		8.3421 (6)	580.53 (11)	
1.67 (10)		8.3301 (10)	578.02 (20)	
2.59 (10)		8.3202 (9)	575.96 (18)	
4.07 (10)		8.2991 (12)	571.61 (26)	
5.46 (13)		8.2878 (13)	569.28 (28)	
0.44 (2)		0.0001 (0)	8.3819 (2)	588.87 (2)
0.44 (2)	0.71 (5)	8.3642 (6)	585.14 (12)	
	2.47 (5)	8.3400 (5)	580.09 (10)	
	3.79 (5)	8.3204 (6)	576.00 (11)	
	4.57 (9)	8.3115 (8)	574.16 (15)	
	5.30 (5)	8.3002 (8)	571.83 (15)	
	6.35 (6)	8.2877 (9)	569.25 (17)	
	7.35 (5)	8.2783 (6)	567.32 (11)	
	8.14 (10)	8.2690 (10)	565.40 (21)	
	9.14 (12)	8.2557 (11)	562.69 (24)	
	10.33 (9)	8.2367 (15)	558.80 (32)	
	0.61 (2)	0.0001 (0)	8.4062 (2)	593.68 (2)
0.40 (5)		8.3974 (8)	592.15 (16)	
1.40 (5)		8.3758 (9)	587.60 (19)	
2.53 (5)		8.3613 (12)	584.56 (26)	
3.61 (9)		8.3471 (7)	581.56 (15)	
4.66 (6)		8.3331 (7)	578.65 (14)	
5.84 (15)		8.3196 (7)	575.84 (14)	
0.77 (2)		0.0001 (0)	8.4214 (1)	597.24 (1)
1.00 (26)		8.4124 (7)	595.32 (14)	
2.12 (10)		8.3865 (9)	589.84 (19)	
3.18 (10)		8.3679 (10)	585.95 (21)	
4.10 (10)	8.3627 (12)	584.84 (26)		
5.46 (10)	8.3466 (9)	581.46 (19)		
6.38 (10)	8.3361 (10)	579.28 (20)		
7.56 (10)	8.3265 (12)	577.29 (26)		
1.00 (0)	0.0001 (0)	8.4393 (1)	601.07 (1)	
	1.62 (10)	8.4277 (15)	598.59 (32)	
	2.50 (10)	8.4138 (13)	595.64 (29)	
	3.60 (10)	8.3947 (9)	591.57 (18)	
	6.90 (10)	8.3414 (15)	580.38 (33)	
	9.12 (11)	8.3217 (13)	576.28 (29)	

^a Data at ambient P and T are from Wang et al. (2012).

^b P in the high- P experiments was determined by averaging the values measured before and after collection of synchrotron data. Fully hydrostatic pressure was potentially not maintained in the experiments, so that a P error of 0.05 GPa was assumed for samples of $x = 0.00$, 0.41 and 0.61 wherever the measured P error was less than 0.05 GPa, and a P error of 0.1 GPa was assumed for samples of $x = 0.22$, 0.77 and 1.00 wherever the measured P error was less than 0.1 GPa.

^c Number in the parentheses represents one standard deviation in the rightmost digit.

The assumption of $K'_T = 4$ for the $\text{MgCr}_2\text{O}_4\text{-Sp}$ is sound. The K'_T value was experimentally determined as either 7.2 (3) (Yong et al., 2012) or 5.8 (4) (Nestola et al., 2014), with the former generally influenced by the non-hydrostatic condition in

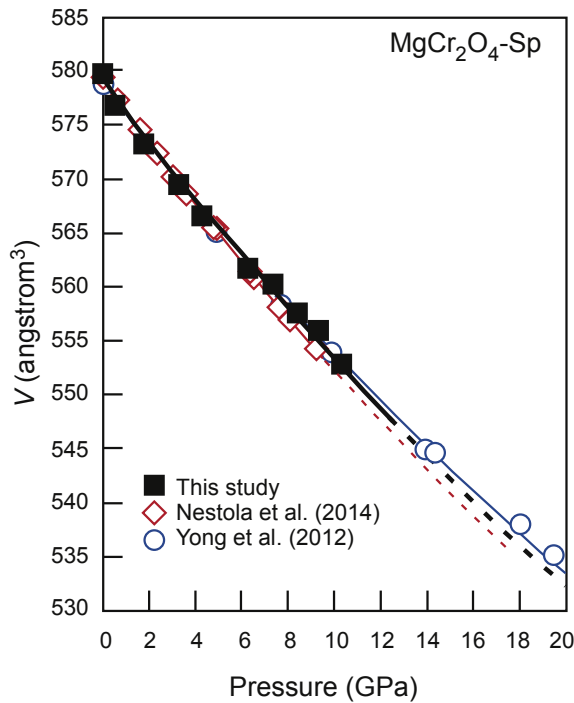


Fig. 1. V – P relations for the MgCr_2O_4 – Sp from different experimental studies (ambient T). Curves are drawn according to the regressed BM-EoS parameters, as listed in Table 2 (with K'_T set at 4). For most data, their error bars are equal to or smaller than the symbols.

the DAC experiments whereas the latter inadequately accurately determined by the limited volume reduction in the high- P experiments ($\sim 4.33\%$, similar to what we achieved in this study). In contrast, early theoretical simulations with variant methods constrained the K'_T value as 3.94 (Catti et al., 1999) or 4.066 (Ottonello et al., 2007). Furthermore, recent first-principles calculations with the CASTEP code using density functional theory and planewave pseudopotential technique, carried out up to 19 GPa by Zhang et al. (2016), generated

similar K'_T values, 4.41 (6) (the exchange–correlation interaction treated with the generalized gradient approximation; GGA) and 4.5 (1) (the exchange–correlation interaction treated with the local density approximation; LDA). It is thus clear that the K'_T values for the MgCr_2O_4 – Sp must be close to 4.

Using our P – V data for the MgCr_2O_4 – Sp (Table 1) and with the assumption of $K'_T = 4$, we have obtained the following BM-EoS parameters: $V_0 = 579.33$ (4) \AA^3 and $K_T = 198.2$ (36) GPa. If we assumed $K'_T = 4.45$, a value averaged from the results reported by Zhang et al. (2016), we would have obtained essentially identical values for the BM-EoS parameters: $V_0 = 579.33$ (4) \AA^3 and $K_T = 196.5$ (35) GPa. As shown in Table 2, the K_T value determined in this study is in good agreement with Yong et al. (2012; 207 (2) GPa) and Nestola et al. (2014; 189.6 (7) GPa); compared on the basis of $K'_T = 4$, it is $\sim 4.3\%$ lower than that from Yong et al. (2012) but $\sim 4.5\%$ higher than that from Nestola et al. (2014). This result is well reflected in the comparison of the P – V trends from these different studies, as shown in Fig. 1.

The K_T value determined here, 198.2 (36) GPa, is very much compatible with the results from all available theoretical investigations. Previously, Catti et al. (1999) and Ottonello et al. (2007) constrained its values as 197.3 and 192.56 GPa, respectively (Table 2). Recently, Zhang et al. (2016) predicted that its value should be between 181.4 (48) GPa (GGA; low boundary) and 216.1 (11) GPa (LDA; high boundary).

3.2. Non-monotonic correlation between K_T and x of the $(\text{Mg}_{1-x}\text{Mn}_x)\text{Cr}_2\text{O}_4$ – Sp_{ss}

The P – V data obtained for all other $(\text{Mg}_{1-x}\text{Mn}_x)\text{Cr}_2\text{O}_4$ – Sp_{ss} are compared to those for the MgCr_2O_4 – Sp in Fig. 2, and are similarly processed with equation (1), with the derived EoS parameters listed in Table 2.

The variation of the K_T values with the compositions of the $(\text{Mg}_{1-x}\text{Mn}_x)\text{Cr}_2\text{O}_4$ – Sp_{ss} is illustrated in Fig. 3. As the

Table 2
EoS parameters of $(\text{Mg}_{1-x}\text{Mn}_x)\text{Cr}_2\text{O}_4$ – Sp_{ss} at ambient P and T .

x	K_T (GPa)	K'_T ^a	V_0 (\AA^3)	Experimental details ^b	Data source ^c
0.00 (0) ^d	207 (2)	4	578.66 (8)	0–19.49; Ar; Gold; Powder	Yong et al. (2012)
0.00 (0)	189 (2)	7.2 (3)	578.68 (4)	0–19.49; Ar; Gold; Powder	Yong et al. (2012)
0.00 (0)	189.6 (7)	4	579.16 (5)	0–9.20; EM; Quartz; SC	Nestola et al. (2014)
0.00 (0)	182.5 (14)	5.8 (4)	579.30 (4)	0–9.20; EM; Quartz; SC	Nestola et al. (2014)
0.00 (0)	198.2 (36)	4	579.33 (4)	0–10.32; EM; Ruby; Powder	This study
0.20 (0)	187.8 (87)	4	583.83 (2)	0–5.46; EM; Ruby; Powder	This study
0.44 (2)	176.1 (32)	4	588.85 (7)	0–10.33; EM; Ruby; Powder	This study
0.61 (2)	168.7 (52)	4	593.67 (5)	0–5.84; EM; Ruby; Powder	This study
0.77 (2)	192.9 (61)	4	597.24 (3)	0–7.56; EM; Ruby; Powder	This study
1.00 (0)	199.2 (106)	4	601.07 (4)	0–9.12; EM; Ruby; Powder	This study

^a Where the K'_T value is not 4, it has been constrained by the P – V data; otherwise, it has been fixed as 4.

^b All compression experiments were done with the DAC, with some of the experimental details listed in the following order: P range (GPa); P medium; P scale; XRD method. Ar, pressure medium of argon; EM, pressure medium of an 1:4 ethanol-methanol mixture; Gold, pressure scale of gold (Fei et al., 2007); Quartz, pressure scale of quartz (Angel et al., 1997); Ruby, pressure scale of ruby (Mao et al., 1978); Powder, powder XRD; SC, single crystal XRD.

^c All samples were synthesized at 1 atm, and either at 1200 °C (Nestola et al., 2014; This study) or 1300 °C (Yong et al., 2012).

^d Number in parentheses represents one standard deviation to the rightmost digit.

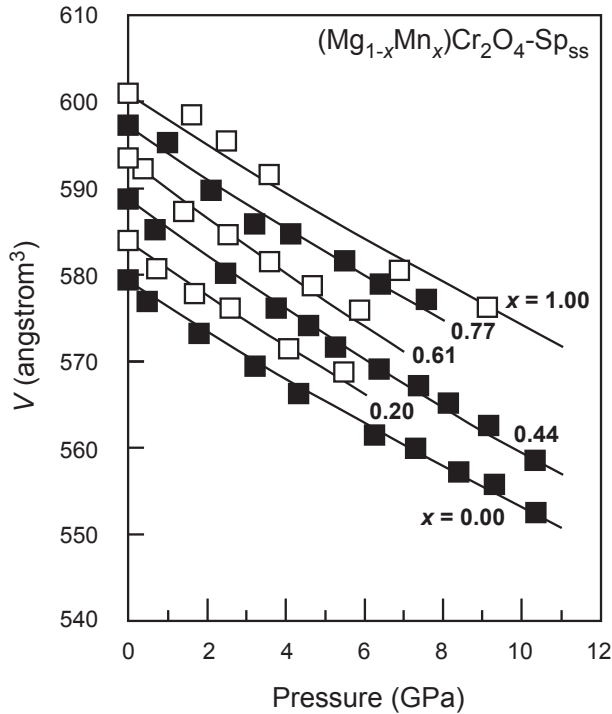


Fig. 2. V - P relations for the $(\text{Mg}_{1-x}\text{Mn}_x)\text{Cr}_2\text{O}_4\text{-Sp}_{\text{ss}}$ observed in this study (ambient T). Curves are drawn according to the regressed BM-EoS parameters, as listed in Table 2 (with K'_T set at 4). For most data, their error bars are equal to or smaller than the symbols.

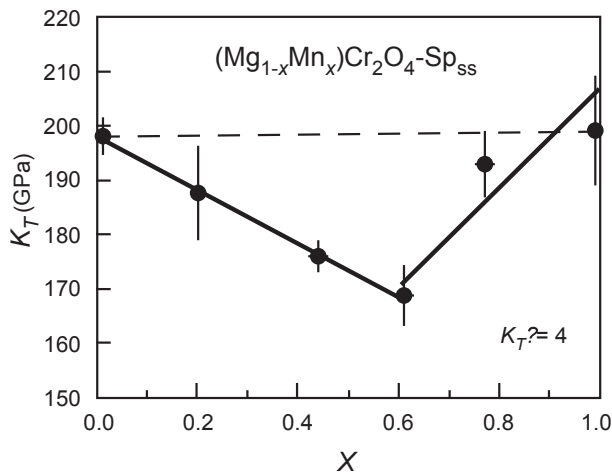


Fig. 3. Correlations between the K_T and x of the $(\text{Mg}_{1-x}\text{Mn}_x)\text{Cr}_2\text{O}_4\text{-Sp}_{\text{ss}}$ (ambient P and T). Data at $x = 0$ and 1 are slightly shifted horizontally to display them more clearly. The broken line was drawn according to equations (5) and (6) in Stixrude and Lithgow-Bertelloni (2005), with the data for the two end-members from this study.

substitution of Mn for Mg progresses, the K_T value first decreases and later increases, with a minimum value of ~ 168.7 (52) approximately at $x = 0.61$. This non-monotonic correlation can be arithmetically described by the following two equations (determined with a weighted linear-squares method):

$$K_T = -49.2(11)x + 198.0(4) \quad (x \leq 0.61), \quad (2)$$

and

$$K_T = 92(41)x + 115(30) \quad (x \geq 0.61). \quad (3)$$

Evidently in Fig. 3, our K_T values for the intermediate compositions between the two end-members $\text{MgCr}_2\text{O}_4\text{-Sp}$ and $\text{MnCr}_2\text{O}_4\text{-Sp}$ are significantly different to those estimated with the assumption of an almost linear compositional dependence (Stixrude and Lithgow-Bertelloni, 2005).

The assumption of a constant K'_T value of 4 for the $(\text{Mg}_{1-x}\text{Mn}_x)\text{Cr}_2\text{O}_4\text{-Sp}_{\text{ss}}$ may be arguable and might affect our major findings here (equations (2) and (3)). It should be recognized that this assumption could not be critically evaluated by our experimental data due to the limited volume reductions achieved in this study. Existent investigations on other series of Sp_{ss} with identical experimental techniques, however, have suggested nearly constant K'_T values. Just to mention a few examples, the K'_T values of the $\text{MgCr}_2\text{O}_4\text{-Sp}$ and $\text{FeCr}_2\text{O}_4\text{-Sp}$ are almost identical (5.8 (4) and 6.1 (5), respectively; Nestola et al., 2014), those of the $\text{MgAl}_2\text{O}_4\text{-Sp}$ with different degrees of cation order are generally the same (5.6 (3) and 5.4 (3); Nestola et al., 2007), and those of the $(\text{Mg}_{1-x}\text{Fe}_x)_2\text{SiO}_4\text{-Sp}_{\text{ss}}$ (ringwoodites) are essentially constant (4.4 (2) for the investigated composition range $x \leq 0.5$; Higo et al., 2006). In contrast, the K'_T values for one certain Sp_{ss} determined in different experimental investigations can be very different, for example 7.2 (3) by Yong et al. (2012) and 5.8 (4) by Nestola et al. (2014) for the $\text{MgCr}_2\text{O}_4\text{-Sp}$, which was mostly caused by different experimental techniques (pressure media, pressure scales, pressure ranges, etc.) and different sample qualities.

Nevertheless, available theoretical investigation conducted with identical techniques simultaneously on both the $\text{MgCr}_2\text{O}_4\text{-Sp}$ and the $\text{MnCr}_2\text{O}_4\text{-Sp}$ indeed suggested some small fluctuation in the K'_T values, from 3.94 for the $\text{MgCr}_2\text{O}_4\text{-Sp}$ to 3.67 for the $\text{MnCr}_2\text{O}_4\text{-Sp}$ (Catti et al., 1999; Quantum-mechanical calculations conducted with the periodic unrestricted Hartree-Fock approach). According to Liu et al. (2016), this level of fluctuation may lead to an uncertainty of < 5 GPa in the K_T , and is therefore unimportant. Consequently, it has to be concluded that the non-monotonic correlation between the K_T values and the compositions of the $(\text{Mg}_{1-x}\text{Mn}_x)\text{Cr}_2\text{O}_4\text{-Sp}_{\text{ss}}$, with the K_T values decreasing by ~ 30 GPa from the two end-members (198.2 (36) GPa for the $\text{MgCr}_2\text{O}_4\text{-Sp}$ and 199.2 (61) GPa for the $\text{MnCr}_2\text{O}_4\text{-Sp}$) towards the intermediate compositions (168.7 (52) GPa for the $(\text{Mg}_{1-x}\text{Mn}_x)\text{Cr}_2\text{O}_4\text{-Sp}$ with $x = 0.61$ (2) for example), must be real.

3.3. Origin of the non-monotonic correlation between K_T and x of the $(\text{Mg}_{1-x}\text{Mn}_x)\text{Cr}_2\text{O}_4\text{-Sp}_{\text{ss}}$

The isothermal bulk moduli of a group of pure compounds (or end-members for complex solid solutions) with the same crystal structure are strongly dependent on their volumes (Anderson and Nafe, 1965). As proposed by Anderson and

Anderson (1970), a relationship of $K_T V_0 = \text{constant}$ holds for the end-members of the Sp group, which implies a monotonic correlation between the K_T and V_0 . For a series of solid solutions such as the $(\text{Mg}_{1-x}\text{Mn}_x)\text{Cr}_2\text{O}_4\text{-Sp}_{\text{ss}}$ along a binary system, the intermediate structures should be more or less strained, so that they do not necessarily follow the same pattern as the end-members do, which is clearly demonstrated here by the non-monotonic correlation between the K_T and x of the $(\text{Mg}_{1-x}\text{Mn}_x)\text{Cr}_2\text{O}_4\text{-Sp}_{\text{ss}}$ (Fig. 3). Recently, similar phenomenon was observed for the $(\text{Mg}_{1-x}\text{Ca}_x)_3\text{Al}_2\text{Si}_3\text{O}_{12}\text{-Gr}_{\text{tss}}$, which show a “W”-shaped compositional dependence of their K_T and thermal expansion coefficient (α_0) at ambient P – T conditions (Du et al., 2015). Note that in both cases the compositional parameter x exerts a monotonic effect on the V_0 (Wang et al., 2012; Du et al., 2015).

For the $(\text{Mg}_{1-x}\text{Mn}_x)\text{Cr}_2\text{O}_4\text{-Sp}_{\text{ss}}$, their V_0 – x data at ambient P and T showed some deviation from the Vegard's law (i.e., ideal mixing; Wang et al., 2012). Here we have further explored their excess mixing volumes ($V_{0\text{-excess}}$) in Fig. 4. With the two end-members attaining zero $V_{0\text{-excess}}$ by definition (hence zero microstrain), the $(\text{Mg}_{1-x}\text{Mn}_x)\text{Cr}_2\text{O}_4\text{-Sp}_{\text{ss}}$ have a third nearly-zero $V_{0\text{-excess}}$ point locating approximately at $x = 0.5$. Additionally, two local $V_{0\text{-excess}}$ maximum points appear at about $x = 0.25$ and $x = 0.75$, which could have been better constrained with more data. Similar $V_{0\text{-excess}}$ – x relationship was also observed for the $\text{Co}(\text{Al}_{1-x}\text{Ga}_x)_2\text{O}_4\text{-Sp}_{\text{ss}}$, with three zero $V_{0\text{-excess}}$ points but one $V_{0\text{-excess}}$ maximum point and one $V_{0\text{-excess}}$ minimum point (Lilova et al., 2010). It follows that the binary Sp_{ss} , with cation substitution either on the tetrahedral sites or on the octahedral sites, may have a rather complicated mixing behavior.

Both the $\text{MgCr}_2\text{O}_4\text{-Sp}$ and the $\text{MnCr}_2\text{O}_4\text{-Sp}$ are 2–3 normal spinel, and the Mg and Mn cations replace each other

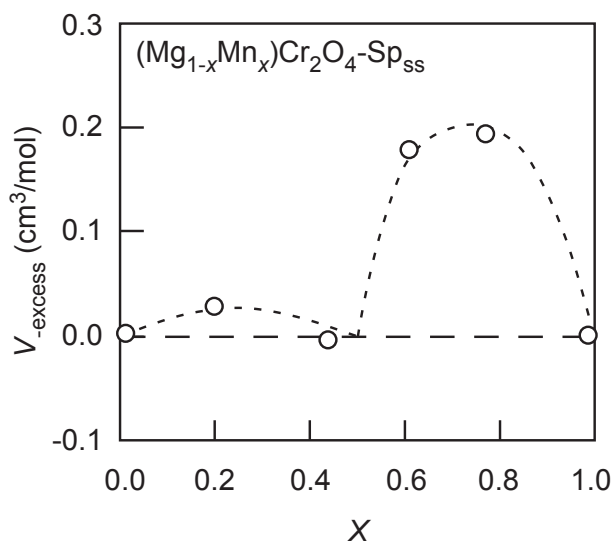


Fig. 4. Relationship between the $V_{0\text{-excess}}$ and x of the $(\text{Mg}_{1-x}\text{Mn}_x)\text{Cr}_2\text{O}_4\text{-Sp}_{\text{ss}}$ (ambient P and T). Data at $x = 0$ and 1 are slightly shifted horizontally to display them more clearly. The broken line was drawn for the case of an ideal mixing whereas the dash line was eye-fitted according to our calculated results.

on the tetrahedral sites of the $(\text{Mg}_{1-x}\text{Mn}_x)\text{Cr}_2\text{O}_4\text{-Sp}_{\text{ss}}$. The size difference between the Mg^{2+} and Mn^{2+} in their fourfold coordination is large, $\sim 12\%$ (O'Neill and Navrotsky, 1983), so that a regular positive mixing behavior may be expected. This would have been broadly confirmed by our observation if we ignored the intermediate part of the $V_{0\text{-excess}}$ – x curve (Fig. 4). Since the Sp_{ss} at about $x = 0.5$ has a nearly-zero $V_{0\text{-excess}}$, its structure should be generally microstrain-free, which presumably implies an even and ordered Mg–Mn distribution on the tetrahedral sites. It follows that this Sp_{ss} at about $x = 0.5$ may behave like a “ghost” end-member for the $(\text{Mg}_{1-x}\text{Mn}_x)\text{Cr}_2\text{O}_4\text{-Sp}_{\text{ss}}$.

The Sp structure is completely determined by its two independent cation-anion distances, termed as $d_{\text{T-O}}$ (averaged bond length of the tetrahedron) and $d_{\text{M-O}}$ (averaged bond length of the octahedron) in this study (Hill et al., 1979; O'Neill and Navrotsky, 1983). According to Lenaz et al. (2004) who investigated the $(\text{Mg}_{1-x}\text{Fe}_x)\text{Cr}_2\text{O}_4\text{-Sp}_{\text{ss}}$ with single-crystal X-ray diffraction method, it is appropriate to assume that the $d_{\text{T-O}}$ varies linearly with the x for the $(\text{Mg}_{1-x}\text{Mn}_x)\text{Cr}_2\text{O}_4\text{-Sp}_{\text{ss}}$, $d_{\text{T-O}} = 1.965 + 0.07x$ Å; the radius for the Mg^{2+} , Mn^{2+} and O^{2-} is 0.585, 0.655 and 1.38 Å, respectively (O'Neill and Navrotsky, 1983; Shannon, 1976). The response of the $d_{\text{M-O}}$ to this Mg–Mn substitution can then be calculated with the following equations (Hazen and Yang, 1999),

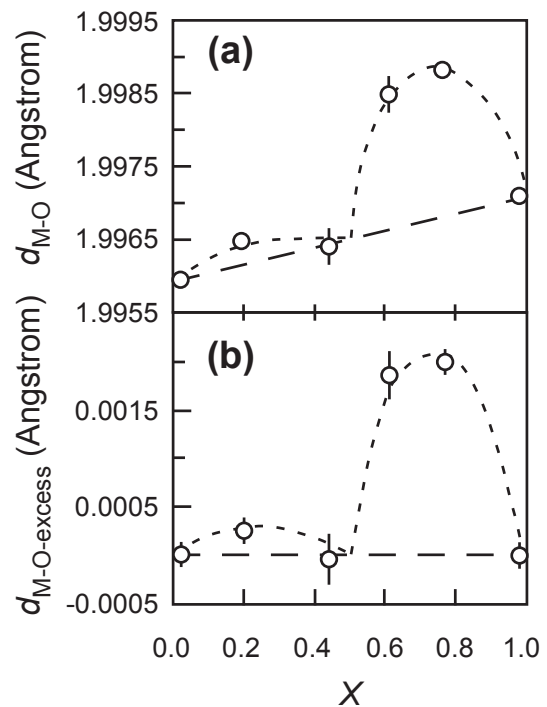


Fig. 5. Correlations between the $d_{\text{M-O}}$ and x (a), and between the $d_{\text{M-O-excess}}$ and x (b) of the $(\text{Mg}_{1-x}\text{Mn}_x)\text{Cr}_2\text{O}_4\text{-Sp}_{\text{ss}}$ (ambient P and T). Data at $x = 0$ and 1 are slightly shifted horizontally to display them more clearly. The broken lines represent the case of an ideal mixing whereas the dash lines were eye-fitted according to our calculated results.

$$d_{M-O} = \sqrt{\frac{A + 8d_{T-O}^2}{33}}, \quad (4)$$

where

$$A = \left(\frac{11\sqrt{3}a - 40d_{T-O}}{8} \right)^2. \quad (5)$$

The result is shown in Fig. 5. As the substitution of Mg by Mn progresses, the d_{M-O} firstly increases gradually up to about $x = 0.25$, secondly remains generally constant for the x interval of ~ 0.25 – 0.5 , then increases quickly up to about $x = 0.75$, and finally decreases gradually towards $x = 1$. In contrast, the d_{M-O} of the $(Mg_{1-x}Fe_x)Cr_2O_4$ – Sp_{ss} remains nearly constant (Lenaz et al., 2004), presumably mainly because the size difference of the Mg^{2+} and Fe^{2+} cations is much smaller (0.585 versus 0.615 Å, or $\sim 5.1\%$ only; O'Neill and Navrotsky, 1983).

This complicated variation pattern of the d_{M-O} , combined with the assumed linear relationship between the d_{T-O} and x , can at least qualitatively explain the non-monotonic correlation between the K_T and x of the $(Mg_{1-x}Mn_x)Cr_2O_4$ – Sp_{ss} (Fig. 3). For the composition interval from $x = 0$ to about $x = 0.75$, both the d_{M-O} and d_{T-O} generally increase, and the M–O and T–O bonds become weaker and hence more compressible, leading to smaller K_T values for the $(Mg_{1-x}Mn_x)Cr_2O_4$ – Sp_{ss} with $x = 0.20(2)$, $0.44(2)$ and $0.61(2)$ (Table 2). For the composition interval from about $x = 0.75$ to $x = 1$, however, the d_{M-O} generally decreases whereas the d_{T-O} continuously increases, suggesting stronger M–O bonds but weaker T–O bonds. Since the number of the M–O bonds is three times that of the T–O bonds in the Sp structure, the role of the M–O bonds dominates the composition range from about $x = 0.75$ to $x = 1$, and results in increasing K_T values for the $(Mg_{1-x}Mn_x)Cr_2O_4$ – Sp_{ss} with $x = 0.77(2)$ and $1.00(0)$ (Table 2). To quantitatively finalize all the details, more measurements on the $(Mg_{1-x}Mn_x)Cr_2O_4$ – Sp_{ss} with different compositions are deemed necessary.

Following the same reasoning, the combined effect of the linear correlation between the d_{T-O} and x and the constant d_{M-O} suggested by Lenaz et al. (2004) for the $(Mg_{1-x}Fe_x)Cr_2O_4$ – Sp_{ss} may result in a nearly linear relationship between the K_T and x , with a slope which may be too small for any high- P experimental investigations. Indeed, Nestola et al. (2014) investigated the $MgCr_2O_4$ – Sp and $FeCr_2O_4$ – Sp with identical experimental techniques, and reached similar K_T values (182.5 (14) GPa with $K'_T = 5.8$ (4) and 184.8 (17) GPa with $K'_T = 6.1$ (5), respectively). The intermediate compositions of the $(Mg_{1-x}Fe_x)Cr_2O_4$ – Sp_{ss} should have similar K_T as well.

3.4. Thermal expansivities of the $(Mg_{1-x}Mn_x)Cr_2O_4$ – Sp_{ss} : a reinterpretation

The thermal expansivity of the $(Mg_{1-x}Mn_x)Cr_2O_4$ – Sp_{ss} was experimentally investigated by Wang et al. (2012) at room P and up to 1000 °C, and a linear correlation between the α_0

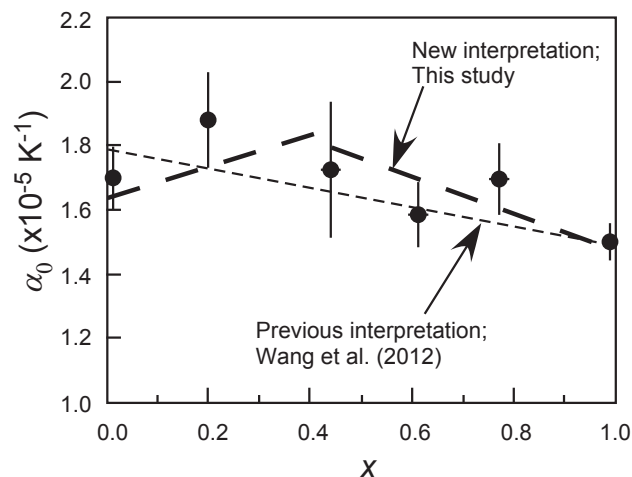


Fig. 6. Correlations between the α_0 and x of the $(Mg_{1-x}Mn_x)Cr_2O_4$ – Sp_{ss} (ambient P and T). Data at $x = 0$ and 1 are slightly shifted horizontally to display them more clearly. Data source: Wang et al. (2012).

and x at ambient P and T was suggested (Fig. 6). In light of the non-monotonic correlation between the K_T and x observed in this study, this linear relationship needs a new interpretation. Due to the relatively small volume variations observed in Wang et al. (2012; up to $\sim 2.40\%$ only), the thermal expansion coefficients should have been less well constrained than the K_T . Note that the volume variations accomplished in this study were much larger, $\sim 5.11\%$ (Table 1).

In general, a compound easy to be compressed at high P should be ready to expand at high T , which roots in the toughness of the constituent chemical bonds. Consequently, the correlation between the α_0 and x is expected to be approximately opposite to that of the K_T and x for one certain series of solid solutions. A careful rescruiting of the experimental result of Wang et al. (2012) indeed suggests a possible kink for the α_0 – x curve, somehow at about $x = 0.44$ rather than at $x = 0.61$ (for the K_T case), with a small increase for the approximately first half of the compositional range but a small decrease for the second half (Fig. 6). A different kink position at about $x = 0.44$ may partially reflect the relatively low accuracy of the α_0 , and partially indicate the necessity of more experimental measurements. Alternatively, the difference of the kink positions may simply be real. The thermal expansivity probes the anharmonicity of the interatomic potential whereas the compressibility probes the entire potential in the region where repulsion begins to dominate, so that the K_T – x curve and the α_0 – x curve for a series of solid solutions need not be exactly opposite to each other (Navrotsky, 1994). For instance, the order of the K_T and α_0 of the isochemical minerals kyanite, andalusite and sillimanite are kyanite > sillimanite > andalusite and andalusite > kyanite > sillimanite, respectively, indicating not exactly opposite roles of T and P on mineral structures (Hu et al., 2011).

Similarly, He et al. (2011, 2012) observed a generally opposite relationship between the α_0 – x curve and the K_T – x

curve for the solid solutions between the lead fluorapatite and lead fluorvanadate apatite ($\text{Pb}_{10}[(\text{PO}_4)_{1-x}(\text{VO}_4)_x]_6\text{F}_2\text{-Ap}_{\text{ss}}$): as x increases from zero to one, the α_0 linearly increases by $\sim 13.4\%$ whereas the K_T linearly decreases by $\sim 16.4\%$. Furthermore, Tribaudino et al. (2008) and Nestola et al. (2008) observed a generally opposite relationship between the α_0 - x curve and the K_T - x curve for the solid solutions between the jadeite and hedenbergite ($(\text{Na}_{1-x}\text{Al}_{1-x})(\text{Ca}_x\text{Fe}_x)\text{Si}_2\text{O}_6$): as x increases from zero to one, the α_0 monotonically increases by $\sim 15\%$ whereas the K_T monotonically decreases by $\sim 23.1\%$. In contrast, Du et al. (2015) observed subparallel, rather than opposite, “W”-shaped α_0 - x curve and K_T - x curve for the $(\text{Mg}_{1-x}\text{Ca}_x)_3\text{Al}_2\text{Si}_3\text{O}_{12}\text{-Grt}_{\text{ss}}$. More investigation on the $(\text{Mg}_{1-x}\text{Ca}_x)_3\text{Al}_2\text{Si}_3\text{O}_{12}\text{-Grt}_{\text{ss}}$ seems favorable.

3.5. Variations of u parameters and component polyhedra of the $(\text{Mg}_{1-x}\text{Mn}_x)\text{Cr}_2\text{O}_4\text{-Sp}_{\text{ss}}$

The primary feature of the Sp structure is a cubic close packing array of the oxygens. The positions of the oxygens are determined by the oxygen parameter u , which reflects the adjustment of the Sp structure to different cation substitutions on the tetrahedral and octahedral sites (Hill et al., 1979). The u parameter can be calculated with the following equation:

$$u = \frac{R^2/4 - 2/3 + (11R^2/48 - 1/18)^{1/2}}{2R^2 - 2}, \quad (6)$$

where R is the ratio of $d_{\text{M-O}}/d_{\text{T-O}}$; it attains the value of 0.25 for an ideal cubic close packing oxygen array. For the $(\text{Mg}_{1-x}\text{Mn}_x)\text{Cr}_2\text{O}_4\text{-Sp}_{\text{ss}}$, the calculated u gradually increases from ~ 0.2611 to 0.2642 as the substitution of Mg by Mn proceeds (Fig. 7a), suggesting that the oxygens move farther away from the nearest tetrahedral Mg^{2+} (or Mn^{2+}) along the [111] direction and their close packing arrangement is more distorted. In detail, however, this distortion is not strictly proportional to the magnitude of the Mg–Mn substitution, but shows some retardance to the compositional change, as indicated by the generally negative u_{excess} values in Fig. 7b. The u_{excess} - x curve is evidently divided into two parts by the $(\text{Mg}_{1-x}\text{Mn}_x)\text{Cr}_2\text{O}_4\text{-Sp}_{\text{ss}}$ with approximately $x = 0.5$, or the “ghost” end-member, which shows a nearly zero u_{excess} value and has a relatively relaxed structure. The negativity of the u_{excess} - x curve for the $(\text{Mg}_{1-x}\text{Mn}_x)\text{Cr}_2\text{O}_4\text{-Sp}_{\text{ss}}$ with $x < 0.5$ is small, implying a small capability accommodating the structural deformation caused by the Mg–Mn substitution. In comparison, the negativity of the u_{excess} - x curve for the $(\text{Mg}_{1-x}\text{Mn}_x)\text{Cr}_2\text{O}_4\text{-Sp}_{\text{ss}}$ with $x > 0.5$ is much larger, suggesting that large structural deformation caused by the Mg–Mn substitution can be readily absorbed. This contrast is understandable because a larger cation (Mn^{2+}) is more difficult to replace a smaller cation (Mg^{2+}) on sites dominated by the smaller cation ($x < 0.5$) than a smaller cation (Mg^{2+}) to replace a larger cation (Mn^{2+}) on sites dominated by the larger cation ($x > 0.5$).

The polyhedra in the Sp structure extensively share their edges in three dimensions, but have very different physical properties (K_T for example; Hazen and Yang, 1999; Zhang et al., 2016), so that they may have extensive but nonuniform responses to the compositional variation along a binary Sp_{ss} . Following Gracia et al. (2002), Zhang et al. (2016) fully decomposed the entire unit cell of the $\text{MgCr}_2\text{O}_4\text{-Sp}$ into five types of polyhedra without introducing any volumetric overlapping, MgO_4 , $(\text{O}_4)_1$, $(\text{O}_4)_2$, CrO_6 and O_6 with multiplicities 8, 8, 48, 16 and 16, respectively. They further calculated the volumes of these component polyhedra using the following equations (Yamanaka and Takéuchi, 1983):

$$V_{\text{MgO}_4} = 64V \cdot |u_{18}|^3/3, \quad (7)$$

$$V_{(\text{O}_4)_1} = 64V \cdot |u_{38}|^3/3, \quad (8)$$

$$V_{(\text{O}_4)_2} = 8V \cdot |u_{18}| \cdot |u_{38}|/3, \quad (9)$$

$$V_{\text{CrO}_6} = 128V \cdot u \cdot u_{38}^2/3, \quad (10)$$

and

$$V_{\text{O}_6} = 128V \cdot u_{18}^2 \cdot |u_{12}|/3, \quad (11)$$

where

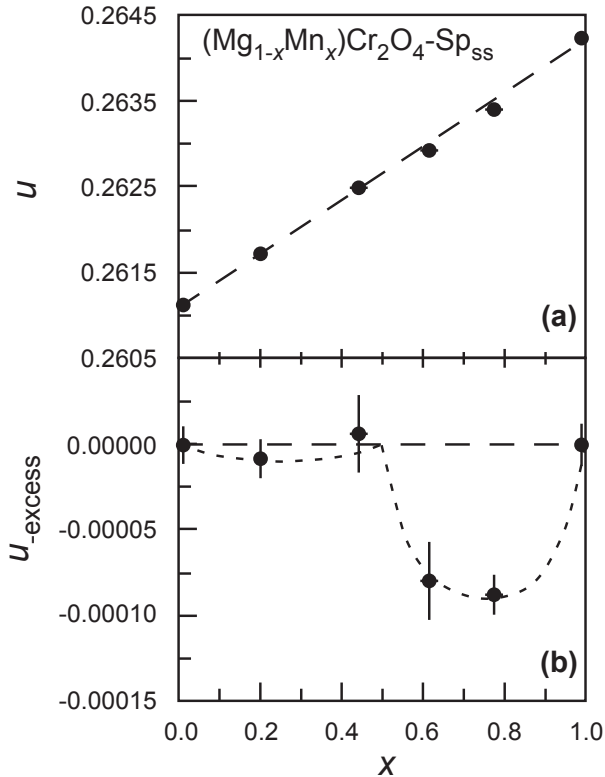


Fig. 7. Correlations between the u and x (a), and between the u_{excess} and x (b) for the $(\text{Mg}_{1-x}\text{Mn}_x)\text{Cr}_2\text{O}_4\text{-Sp}_{\text{ss}}$ (ambient P and T). Data at $x = 0$ and 1 are slightly shifted horizontally to display them more clearly. The broken line in (a) and (b) represents an ideal evolution of the u and u_{excess} , respectively. The dash line in (b) was eye-fitted according to our calculated results.

$$u_{ij} = u - i/j. \quad (12)$$

Similarly, we have carried out the calculations for the $(\text{Mg}_{1-x}\text{Mn}_x)\text{Cr}_2\text{O}_4\text{-Sp}_{\text{ss}}$. The results show that the volume percentages for the five types of polyhedra MgO_4 , $(\text{O}_4)_1$, $(\text{O}_4)_2$, CrO_6 and O_6 in the $\text{MgCr}_2\text{O}_4\text{-Sp}$ structure are ~5.4, 3.2, 24.8, 28.9 and 37.8%, respectively. As the Mg–Mn substitution proceeds and accomplishes, the volume changes of these five types of polyhedra in the unit cells of the $(\text{Mg}_{1-x}\text{Mn}_x)\text{Cr}_2\text{O}_4\text{-Sp}_{\text{ss}}$ are not uniform indeed: the volume of the $(\text{Mg,Mn})\text{O}_4$ increases by ~7.1% (from 31.15 to 34.60 \AA^3), that of the $(\text{O}_4)_1$ decreases by ~8.0% (from 18.27 to 17.43 \AA^3), that of the $(\text{O}_4)_2$ remains almost constant (reduced by ~0.5%; from 143.70 to 148.32 \AA^3), that of the CrO_6 decreases by ~4.3% (from 167.48 to 166.32 \AA^3), and that of the O_6 increases by ~3.3% (from 218.74 to 234.39 \AA^3). On the other hand, the total volume of the tetrahedra MgO_4 , $(\text{O}_4)_1$ and $(\text{O}_4)_2$ increases by 3.75% (from 193.11 to 200.36 \AA^3), and so does the total volume of the octahedra CrO_6 and O_6 (by 3.75% from 386.23 to 400.71 \AA^3). A constant volume ratio of 1:2, as embedded in equations (7)–(11), is therefore maintained between these tetrahedra and these octahedra whatever the deformation extent of the oxygen array is (Fig. 7).

The volumes of the individual polyhedra (V_{poly}) must have different responses to the compositional change as well. The $V_{\text{poly-x}}$ relationships are shown in Fig. 8a–e, and the $V_{\text{poly-excess-x}}$ relationships are shown in Fig. 8a*–e*.

Although volumetrically unimportant, the $(\text{Mg,Mn})\text{O}_4$ tetrahedron shows the largest volume variation, ~11.1% (from 3.894 (4) to 4.325 (4) \AA^3), as x increases from zero to one (Fig. 8a). This is totally expected since the compositional variation of the $(\text{Mg}_{1-x}\text{Mn}_x)\text{Cr}_2\text{O}_4\text{-Sp}_{\text{ss}}$ takes place on the $(\text{Mg,Mn})\text{O}_4$ tetrahedra. In addition, a negative $V_{\text{poly-excess-x}}$ relationship is demonstrated by our results (Fig. 8a*), as dictated by the assumed ideal mixing behavior.

In contrast, the other two types of tetrahedra, $(\text{O}_4)_1$ and $(\text{O}_4)_2$, show completely different behaviors; their $V_{\text{poly-x}}$ relationships and $V_{\text{poly-excess-x}}$ relationships are rather complicated (Fig. 8b and c, and Fig. 8b* and c*, respectively). Although their volumes either linearly decrease (by ~4.6% from 2.283 (3) to 2.179 (3) \AA^3 for the $(\text{O}_4)_1$) or increase (by ~3.2% from 2.994 (0) to 3.090 (0) \AA^3 for the $(\text{O}_4)_2$), both types of tetrahedra show generally positive mixing behaviors. In detail, their $V_{\text{poly-excess-x}}$ curves are divided into two parts approximately by the “ghost” end-member, the $(\text{Mg}_{1-x}\text{Mn}_x)\text{Cr}_2\text{O}_4\text{-Sp}_{\text{ss}}$ with $x = 0.5$. Interestingly, the first local maximum positivity is much smaller than the second in both cases, suggesting that the $(\text{Mg}_{1-x}\text{Mn}_x)\text{Cr}_2\text{O}_4\text{-Sp}_{\text{ss}}$ in the compositional range of $0.5 < x < 1$ have much larger compliances to any local strains caused by the Mg–Mn substitution.

The CrO_6 octahedron shows a peculiar volumetric variation (Fig. 8d). Its overall variation is an extremely small reduction (~0.7% from 10.468 (6) to 10.395 (6) \AA^3), which is mostly expected due to its relatively large bulk modulus (~230 (30) GPa; Hazen and Finger, 1979). Against this general trend, and interestingly, the volumes of the CrO_6 octahedron in the $(\text{Mg}_{1-x}\text{Mn}_x)\text{Cr}_2\text{O}_4\text{-Sp}_{\text{ss}}$ at $x = 0.61$ (2) and 0.77 (2) are somehow larger than the volume of the CrO_6 octahedron in the $(\text{Mg}_{1-x}\text{Mn}_x)\text{Cr}_2\text{O}_4\text{-Sp}_{\text{ss}}$ at $x = 0.44$ (2). Combined with the general positive correlation between the $d_{\text{M-O}}$ and x (Fig. 5a), the overall negative relationship between the CrO_6 volume and x implies continuous deformation of the CrO_6 octahedron. Furthermore, the $V_{\text{poly-excess-x}}$ curve is much similar to the $d_{\text{M-O-excess-x}}$ curve (Figs. 8d* and 5a). Like in the cases of the $(\text{O}_4)_1$ and $(\text{O}_4)_2$ (Fig. 8b* and c*), the positive $V_{\text{poly-excess-x}}$ curve for the CrO_6 octahedron is divided into two parts by the “ghost” end-member, with the second part much more prominent than the first part.

The volume of the individual O_6 octahedron of the $(\text{Mg}_{1-x}\text{Mn}_x)\text{Cr}_2\text{O}_4\text{-Sp}_{\text{ss}}$ increases significantly, by ~7.2% (from 13.671 (6) to 14.650 (7) \AA^3 ; Fig. 8e). The O_6 octahedron is the second most compressible polyhedra in the $\text{MgCr}_2\text{O}_4\text{-Sp}$ (only less compressible than the MgO_4 tetrahedron; Zhang et al., 2016), and its volumetric variation comes as the second largest. The $V_{\text{poly-excess-x}}$ curve is very interesting, with the first part at $x < 0.5$ negligible whereas the second part at $x > 0.5$ distinctively positive (Fig. 8e*).

In summary, a range of structural adjustments takes place when Mn substitutes for Mg in the $(\text{Mg}_{1-x}\text{Mn}_x)\text{Cr}_2\text{O}_4\text{-Sp}_{\text{ss}}$.

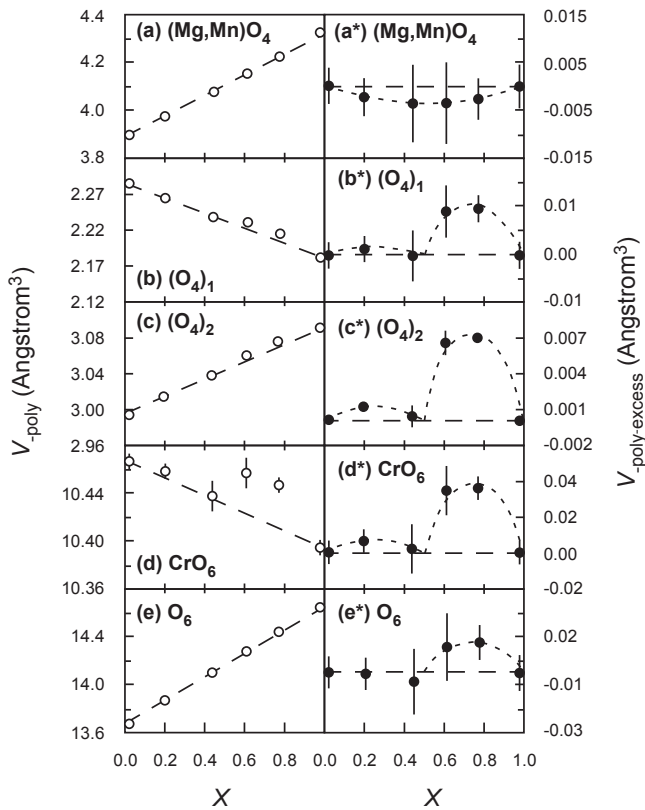


Fig. 8. Correlations between the polyhedral volume (V_{poly}) and x ((a) $(\text{Mg,Mn})\text{O}_4$, (b) $(\text{O}_4)_1$, (c) $(\text{O}_4)_2$, (d) CrO_6 and (e) O_6), and between the $V_{\text{poly-excess}}$ and x ((a*) $(\text{Mg,Mn})\text{O}_4$, (b*) $(\text{O}_4)_1$, (c*) $(\text{O}_4)_2$, (d*) CrO_6 and (e*) O_6) of the $(\text{Mg}_{1-x}\text{Mn}_x)\text{Cr}_2\text{O}_4\text{-Sp}_{\text{ss}}$ (ambient P and T). Data at $x = 0$ and 1 are slightly shifted horizontally to display them more clearly. The broken lines represent ideal mixing whereas the dash lines were eye-fitted according to our calculated results.

As x increases from 0 to 1, the volumes of the unit cell, the tetrahedra (the MgO_4 , $(\text{O}_4)_1$ and $(\text{O}_4)_2$) and the octahedra (the CrO_6 and O_6) increase by similar amounts (i.e., 3.75%). The volume of the individual $(\text{O}_4)_1$ tetrahedron or CrO_6 octahedron decreases in fact (Fig. 8b and d), but is readily over-compensated by the MgO_4 and $(\text{O}_4)_2$ tetrahedra (Fig. 8a and c), or by the O_6 octahedron (Fig. 8e), respectively. The oxygen array continuously deforms further (Fig. 7a). The $(\text{Mg}_{1-x}\text{Mn}_x)\text{Cr}_2\text{O}_4\text{-Sp}_{\text{ss}}$ with $x < 0.5$ have smaller compliance in promoting the Mg–Mn substitution than those with $x > 0.5$, as indicated by the $u_{\text{excess}}\text{-}x$ curve (Fig. 7b) and the $V_{\text{poly-excess}}\text{-}x$ curves (Fig. 8b*–e*).

4. Implication

In order to accurately constrain the chemical composition and geophysical behavior of the interior of the Earth, precise determinations of the K_T for the constituent minerals with relevant compositions are important. With recent rapid development of some experimental techniques, especially the synchrotron-based high- P techniques, a huge body of data with increasing accuracy has been generated. Due to the large variety of the mineral species and the complex of their compositions, some extrapolation or interpolation with the assumption of a generally linear compositional dependence of the K_T is presently still employed in many cases. For such cases, our study implies that great precaution must be taken since the factors affecting the compressional behavior of mineral solid solutions have not been fully understood.

Many factors, including but not limited to the structure feature of the solid solutions (Hazen and Finger, 1979), the size mismatch of the substituting cations (O'Neill and Navrotsky, 1984), their charge difference (Fe^{3+} versus Ti^{4+} in $\text{Fe}_{3-x}\text{Ti}_x\text{O}_4\text{-Sp}_{\text{ss}}$ for example; Yamanaka et al., 2013), and their electronic and magnetic contrast (Mg^{2+} versus Fe^{2+} in $(\text{Mg}_{1-x}\text{Fe}_x)_2\text{SiO}_4\text{-Ol}_{\text{ss}}$ for example; Dachs et al., 2007), can affect the mixing behavior of a solid solution series, affect the K_T , and affect the correlation pattern of the K_T and composition.

For the crystal structures with extensive edge sharing between the component polyhedra, the size mismatch of the substituting cations is important in determining the relationship between the K_T and composition of a series of solid solutions: if the size difference is small, it has a high tendency to be linear; otherwise, it may be complicated. As demonstrated for the Sp structure, the size difference of the Mg^{2+} and Fe^{2+} in the $(\text{Mg}_{1-x}\text{Fe}_x)_2\text{SiO}_4\text{-Sp}_{\text{ss}}$ is relatively small ($\sim 3.5\%$; O'Neill and Navrotsky, 1983), the K_T has an almost linear dependence to the x (Liu et al., 2016). In comparison, the size difference of the Mg^{2+} and Mn^{2+} in the $(\text{Mg}_{1-x}\text{Mn}_x)\text{Cr}_2\text{O}_4\text{-Sp}_{\text{ss}}$ is somewhat large ($\sim 12\%$; O'Neill and Navrotsky, 1983), the K_T and x have a non-monotonic relationship. Similar phenomenon has also been observed for the Grt structure: for the $(\text{Mg}_{1-x}\text{Fe}_x)_3\text{Al}_2\text{Si}_3\text{O}_{12}\text{-Grt}_{\text{ss}}$ ($\sim 3.4\%$ difference in the sizes of the Mg^{2+} and Fe^{2+} ; Shannon, 1976), the correlation between the K_T and x is nearly linear (Huang and Chen, 2014); for the $(\text{Mg}_{1-x}\text{Ca}_x)_3\text{Al}_2\text{Si}_3\text{O}_{12}\text{-Grt}_{\text{ss}}$

($\sim 25.8\%$ difference in the sizes of the Mg^{2+} and Fe^{2+} ; Shannon, 1976), the correlation between the K_T and x is “W”-shaped (Du et al., 2015). This hypothesis seems applicable to the $(\text{Mg}_{1-x}\text{Fe}_x)\text{O}$ periclase-wüstite solid solutions as well, as a generally linear correlation has been observed between the K_T and x (Fei, 1999; an $\sim 3.5\%$ difference in the cation sizes (Shannon, 1976)). For less tightly-bound crystal structures such as the pyroxene and feldspar, on the other hand, the size mismatch of the substituting cations is presumably less important in determining the correlation between the K_T and composition, which is usually monotonic with small curvature. This proposal has been supported by the experimental observations along the $\text{NaAlSi}_2\text{O}_6\text{-CaFeSi}_2\text{O}_6$ join and $\text{NaAlSi}_3\text{O}_8\text{-CaAl}_2\text{Si}_2\text{O}_8$ join which involve substituting cations with a large range of cation size differences (Angel, 2004; Nestola et al., 2008). For the least tightly-bound or open crystal structures like the olivine and apatite, further, the size mismatch of the substituting cations is usually unimportant in determining the correlation between the K_T and composition, which is commonly linear. For example, the size difference of P^{5+} and V^{5+} in the $\text{Pb}_{10}[(\text{PO}_4)_{1-x}(\text{VO}_4)_x]_6\text{-F}_2\text{-Ap}_{\text{ss}}$ is as large as $\sim 108.9\%$ (Shannon, 1976), and the K_T and x relationship has been established as generally linear (He et al., 2012). For the $(\text{Mg}_{1-x}\text{Fe}_x)_2\text{SiO}_4\text{-Ol}_{\text{ss}}$, the cation size difference is small and the K_T and x relationship is linear (Poe et al., 2010; Nestola et al., 2011a, 2011b), matching the expectation.

Other factors like the charge difference, electronic distinction and magnetic contrast are usually associated with the substitution of different cations with different sizes, so that their effects on the correlation pattern between the K_T and composition are hard to separate and much less well constrained experimentally. O'Neill and Navrotsky (1983) had some discussions on the electronic entropy in the transition-metal Sp, and pointed out that the electronic entropy might affect the cation distribution between the tetrahedra and octahedra in a complicated way. Dachs et al. (2007) delicately constrained the electronic and magnetic contributions to the molar entropy of mixing for the $(\text{Mg}_{1-x}\text{Fe}_x)_2\text{SiO}_4\text{-Ol}_{\text{ss}}$, demonstrated their importance, and claimed that they might make the thermodynamic behavior of the Ol_{ss} very complicated. Apparently much more work is required before the effects of these factors on the relationship between the K_T and composition can be adequately understood.

Acknowledgments

The in situ X-ray diffraction experiments were carried out at the National Synchrotron Light Source (NSLS), which is supported by the U.S. Department of Energy, Division of Materials Sciences and Division of Chemical Sciences under Contract No. DE-AC02-76CH00016. The operation of X17C is supported by COMPRES, the Consortium for Materials Properties Research in Earth Sciences. This work is financially supported by the National Natural Science Foundation of China (Grant No. 41273072 and 41440015).

References

- Anderson, D.L., Anderson, O.L., 1970. The bulk modulus-volume relationship for oxides. *J. Geophys. Res.* 75, 3494–3500.
- Anderson, O.L., Nafe, J.E., 1965. The bulk modulus-volume relationship for oxide compounds and related geophysical problems. *J. Geophys. Res.* 70, 3951–3963.
- Angel, R.J., Allan, D.R., Miletich, R., Finger, L.W., 1997. The use of quartz as an internal pressure standard in high-pressure crystallography. *J. Appl. Crystallogr.* 30, 461–466.
- Angel, R.J., 2004. Equations of state of plagioclase feldspars. *Contrib. Mineral. Petrol.* 146, 506–512.
- Birch, F., 1947. Finite elastic strain of cubic crystals. *Phys. Rev.* 71, 809–924.
- Cammarano, F., Goes, S., Deuss, A., Giardini, D., 2005a. Is a pyrolytic adiabatic mantle compatible with seismic data? *Earth Planet. Sci. Lett.* 232, 227–243.
- Cammarano, F., Deuss, A., Goes, S., Giardini, D., 2005b. One-dimensional physical reference models for the upper mantle and transition zone: combining seismic and mineral physics constraints. *J. Geophys. Res.* 110, B01306.
- Catti, M., Freyria Fava, F., Zicovich, C., Dovesi, R., 1999. High-pressure decomposition of MgCr_2O_4 spinels ($M=\text{Mg, Mn, Zn}$) by ab initio methods. *Phys. Chem. Miner.* 26, 389–395.
- Chang, L., Chen, Z., Liu, X., Wang, H., 2013. Expansivity and compressibility of wadeite-type $\text{K}_2\text{Si}_4\text{O}_9$ determined by in situ high T/P experiments, and their implication. *Phys. Chem. Miner.* 40, 29–40.
- Dachs, E., Geiger, C.A., von Seckendorff, V., Grodzicki, M., 2007. A low-temperature calorimetric study of synthetic (forsterite + fayalite) $\{(\text{Mg}_2\text{SiO}_4 + \text{Fe}_2\text{SiO}_4)\}$ solid solutions: an analysis of vibrational, magnetic, and electronic contributions to the molar heat capacity and entropy of mixing. *J. Chem. Thermodyn.* 39, 906–933.
- Deng, L., Liu, X., Liu, H., Dong, J., 2010. High-pressure phase relations in the composition of albite $\text{NaAlSi}_3\text{O}_8$ constrained by an ab initio and quasi-harmonic Debye model, and their implications. *Earth Planet. Sci. Lett.* 298, 427–433.
- Duffy, T.S., Wang, Y., 1998. Pressure-volume-temperature equations of state. In: Hemley, R.J. (Ed.), *Ultra-high-pressure Mineralogy*, vol. 37. Reviews in Mineralogy, Mineralogical Society of America, Washington, pp. 425–457.
- Du, W., Clark, S.M., Walker, D., 2015. Thermo-compression of pyrope-grossular garnet solid solutions: non-linear compositional dependence. *Am. Mineral.* 100, 215–222.
- Fei, Y., Mao, H.-K., 1993. Static compression of $\text{Mg}(\text{OH})_2$ to 78 GPa at high temperatures and constraints on the equation of state of fluid H_2O . *J. Geophys. Res.* 98, 11875–11884.
- Fei, Y., 1999. Effects of temperature and composition on the bulk modulus of $(\text{Mg,Fe})\text{O}$. *Am. Mineral.* 84, 272–276.
- Fei, Y., Ricolleau, A., Frank, M., Mibe, K., Shen, G., Prakapenka, V., 2007. Toward an internally consistent pressure scale. *Proc. Natl. Acad. Sci. U. S. A.* 104, 9182–9186.
- Gilewicz-Wolter, J., Zurek, Z., Dudala, J., Lis, J., Homa, M., Wolter, M., 2005. Diffusion of chromium, manganese, and iron in MnCr_2O_4 spinel. *J. Phase Equilib. Diff.* 26, 561–564.
- Gracia, L., Beltrán, A., Andrés, J., Franco, R., Recio, J.M., 2002. Quantum-mechanical simulation of MgAl_2O_4 under high pressure. *Phys. Rev. B* 66, 224114.
- Graham, J., 1978. Manganochromite, palladium antimonide, and some unusual mineral associations at the Nairne pyrite deposit, South Australia. *Am. Mineral.* 63, 1166–1174.
- Hammersley, J., 1996. Fit2D report. Europe Synchrotron Radiation Facility, France, Grenoble.
- Hazen, R.M., Finger, L.W., 1979. Bulk modulus-volume relationship for cation-anion polyhedra. *J. Geophys. Res.* 84, 6273–6278.
- Hazen, R.M., 1993. Comparative compressibilities of silicate spinels: anomalous behavior of $(\text{Mg,Fe})_2\text{SiO}_4$. *Science* 259, 206–209.
- Hazen, R.M., Yang, H., 1999. Effects of cation substitution and order-disorder on P-V-T equations of state of cubic spinels. *Am. Mineral.* 84, 1956–1960.
- He, Q., Liu, X., Hu, X., Li, S., Wang, H., 2011. Solid solution between lead fluoapatite and lead fluorvanadate apatite: mixing behavior, Raman feature and thermal expansivity. *Phys. Chem. Miner.* 38, 741–752.
- He, Q., Liu, X., Hu, X., Deng, L., Chen, Z., Li, B., Fei, Y., 2012. Solid solutions between lead fluorapatite and lead fluorvanadate apatite: compressibility determined by using a diamond-anvil cell coupled with synchrotron X-ray diffraction. *Phys. Chem. Miner.* 39, 219–226.
- Higo, Y., Inoue, T., Li, B., Irifune, T., Liebermann, R.C., 2006. The effect of iron on the elastic properties of ringwoodite at high pressure. *Phys. Earth Planet. Inter.* 159, 276–285.
- Hill, R.J., Craig, J.R., Gibbs, G.V., 1979. Systematics of the spinel structure type. *Phys. Chem. Miner.* 4, 317–339.
- Huang, S., Chen, J., 2014. Equation of state of pyrope-almandine solid solution measured using a diamond anvil cell and in situ synchrotron X-ray diffraction. *Phys. Earth Planet. Inter.* 228, 88–91.
- Hu, X., Liu, X., He, Q., Wang, H., Qin, S., Ren, L., Wu, C.M., Chang, L., 2011. Thermal expansion of andalusite and sillimanite at ambient pressure: a powder X-ray diffraction study up to 1000 °C. *Mineral. Mag.* 75, 363–374.
- Ishii, T., Kojitani, H., Fujino, K., Yusa, H., Mori, D., Inaguma, Y., Matsushita, Y., Yamaura, K., Akaogi, M., 2015. High-pressure high-temperature transitions in MgCr_2O_4 and crystal structures of new $\text{Mg}_2\text{Cr}_2\text{O}_5$ and post-spinel MgCr_2O_4 phases with implications for ultrahigh-pressure chromitites in ophiolites. *Am. Mineral.* 100, 59–65.
- Ita, J., Stixrude, L., 1992. Petrology, elasticity, and composition of the mantle transition zone. *J. Geophys. Res.* 97, 6849–6866.
- Jackson, J.M., Sinogeikin, S.V., Bass, J.D., 2000. Sound velocities and elastic properties of $\gamma\text{-Mg}_2\text{SiO}_4$ to 873 K by Brillouin spectroscopy. *Am. Mineral.* 85, 296–303.
- Klotz, S., Chervin, J.C., Munsch, P., Le Marchand, G., 2009. Hydrostatic limits of 11 pressure transmitting media. *J. Phys. D Appl. Phys.* 42, 075413.
- Lenaz, D., Skogby, H., Princivalle, F., Hälenius, U., 2004. Structural changes and valence states in the $\text{MgCr}_2\text{O}_4\text{-FeCr}_2\text{O}_4$ solid solution series. *Phys. Chem. Miner.* 31, 633–642.
- Li, B., Liebermann, R.C., Weidner, D.J., 1998. Elasticity of wadsleyite to 7 GPa and 873 kelvin. *Science* 281, 675–677.
- Liebermann, R.C., Jackson, I., Ringwood, A.E., 1977. Elasticity and phase equilibria of spinel disproportionation reactions. *Geophys. J. R. Astronomical Soc.* 50, 553–586.
- Lilova, K.I., Navrotsky, A., Melot, B.C., Seshadri, R., 2010. Thermodynamics of $\text{CoAl}_2\text{O}_4\text{-CoGa}_2\text{O}_4$ solid solutions. *J. Solid State Chem.* 183, 1266–1271.
- Liu, X., O'Neill, H.St.C., 2004. The effect of Cr_2O_3 on the partial melting of spinel lherzolite in the system $\text{CaO-MgO-Al}_2\text{O}_3\text{-SiO}_2\text{-Cr}_2\text{O}_3$ at 1.1 GPa. *J. Petrol.* 45, 2261–2286.
- Liu, X., Shieh, S.R., Fleet, M.E., Zhang, L., 2009. Compressibility of a natural kyanite to 17.5 GPa. *Prog. Nat. Sci.* 19, 1281–1286.
- Liu, X., Shieh, S.R., Fleet, M.E., Zhang, L., He, Q., 2011. Equation of state of carbonated hydroxylapatite at ambient temperature up to 10 GPa: significance of carbonate. *Am. Mineral.* 96, 74–80.
- Liu, X., Ohfuji, H., Nishiyama, N., He, Q., Sanehira, T., Irifune, T., 2012. High-P behavior of anorthite composition and some phase relations of the $\text{CaO-Al}_2\text{O}_3\text{-SiO}_2$ system to the lower mantle of the Earth, and their geophysical implications. *J. Geophys. Res.* 117, B09206.
- Liu, X., Xiong, Z., Chang, L., He, Q., Wang, F., Shieh, S.R., Wu, C., Li, B., Zhang, L., 2016. Anhydrous ringwoodites in the mantle transition zone: their bulk modulus, solid solution behavior, compositional variation, and sound velocity feature. *Solid Earth Sci.* 1, 28–47.
- Mao, H.-K., Takahashi, T., Bassett, W.A., Weaver, J.S., Akimoto, S., 1969. Effect of pressure and temperature on the molar volumes of wüstite and of three $(\text{Fe, Mg})_2\text{SiO}_4$ spinel solid solutions. *J. Geophys. Res.* 74, 1061–1069.
- Mao, H.-K., Bell, P.M., Shaner, J.W., Steinberg, D.J., 1978. Specific volume measurements of Cu, Mo, Pt, and Au and calibration of ruby R1 fluorescence pressure gauge for 0.006 to 1 Mbar. *J. Appl. Phys.* 49, 3276–3283.
- Moriwake, H., Tanaka, I., Oba, F., Koyama, Y., Adachi, H., 2002. Formation energy of Cr/Al vacancies in spinel MgCr_2O_4 and MgAl_2O_4 by first-principles calculations. *Phys. Rev. B* 65, 153103.
- Navrotsky, A., 1994. *Physics and Chemistry of Earth Materials*. Cambridge University Press.

- Nestola, F., Boffa Ballaran, T., Balić-Žunić, T., Princivalle, F., Secco, L., Dal Negro, A., 2007. Comparative compressibility and structural behavior of spinel MgAl_2O_4 at high pressures: the independency on the degree of cation order. *Am. Mineral.* 92, 1838–1843.
- Nestola, F., Boffa Ballaran, T., Liebske, C., Thompson, R., Downs, R.T., 2008. The effect of the hedenbergitic substitution on the compressibility of jadeite. *Am. Mineral.* 93, 1005–1013.
- Nestola, F., Pasqual, D., Smyth, J.R., Novella, D., Secco, L., Manghnani, M.H., Dal Negro, A., 2011a. New accurate elastic parameters for the forsterite-fayalite solid solution. *Am. Mineral.* 96, 1742–1747.
- Nestola, F., Nimis, P., Ziberna, L., Longo, M., Marzoli, A., Harris, J.W., Manghnani, M.H., Fedortchouk, Y., 2011b. First crystal-structure determination of olivine in diamond: composition and implications for provenance in the Earth's mantle. *Earth Planet. Sci. Lett.* 305, 249–255.
- Nestola, F., Periotto, B., Andreozzi, G.B., Bruschini, E., Bosi, F., 2014. Pressure-volume equation of state for chromite and magnesiochromite: a single-crystal X-ray diffraction investigation. *Am. Mineral.* 99, 1248–1253.
- Oganov, A.R., Brodholt, J.P., Price, G.D., 2000. The elastic constants of MgSiO_3 perovskite at pressures and temperatures of the Earth's mantle. *Nature* 404, 934–937.
- O'Neill, H.St.C., Navrotsky, A., 1983. Simple spinels: crystallographic parameters, cation radii, lattice energies, and cation distribution. *Am. Mineral.* 68, 181–194.
- O'Neill, H.St.C., Navrotsky, A., 1984. Cation distribution and thermodynamic properties of binary spinel solid solutions. *Am. Mineral.* 69, 733–753.
- O'Neill, H.St.C., Dollase, W.A., 1994. Crystal structures and cation distributions in simple spinels from powder XRD structural refinements: MgCr_2O_4 , ZnCr_2O_4 , Fe_3O_4 and the temperature dependence of the cation distribution in ZnAl_2O_4 . *Phys. Chem. Miner.* 20, 541–555.
- Ottoneo, G., Civalleri, B., Zuccolini, M.V., Zicovich-Wilson, C.M., 2007. Ab-initio thermal physics and Cr-isotopic fractionation of MgCr_2O_4 . *Am. Mineral.* 92, 98–108.
- Paraskevopoulos, G.M., Economou, M., 1981. Zoned Mn-rich chromite from podiform type chromite ore in serpentinites of northern Greece. *Am. Mineral.* 66, 1013–1019.
- Poe, B.T., Romano, C., Nestola, F., Smyth, J.R., 2010. Electrical conductivity anisotropy of dry and hydrous olivine at 8 GPa. *Phys. Earth Planet. Inter.* 181, 103–111.
- Powell, R., Holland, T.J.B., 1985. An internally consistent thermodynamic dataset with uncertainties and correlations: 1. Methods and a worked example. *J. Metamorph. Geol.* 3, 327–342.
- Raccah, P.M., Bouchard, R.J., Wold, A., 1966. Crystallographic study of chromium spinels. *J. Appl. Phys.* 37, 1436–1437.
- Ricolleau, A., Fei, Y., Cottrell, E., Watson, H., Deng, L., Zhang, L., Fiquet, G., Auzende, A.-L., Roskosz, M., Morard, G., Prakapenka, V., 2009. Density profile of pyrolite under the lower mantle conditions. *Geophys. Res. Lett.* 36, L06302.
- Shannon, R.D., 1976. Revised effective ionic radii and systematic studies of interatomic distances in halides and chalcogenides. *Acta Crystallogr. A* 32, 751–767.
- Shieh, S.R., Duffy, T.S., Kubo, A., Shen, G., Prakapenka, V.B., Sata, N., Hirose, K., Ohishi, Y., 2006. Equation of state of the postperovskite phase synthesized from a natural $(\text{Mg,Fe})\text{SiO}_3$ orthopyroxene. *Proc. Natl. Acad. Sci. U. S. A.* 103, 3039–3043.
- Stefan, E., Irvine, J.T.S., 2011. Synthesis and characterization of chromium spinels as potential electrode support materials for intermediate temperature solid oxide fuel cells. *J. Mater. Sci.* 46, 7191–7197.
- Stixrude, L., Lithgow-Bertelloni, C., 2005. Thermodynamics of mantle minerals – I. Physical properties. *Geophys. J. Int.* 162, 610–632.
- Tribaudino, M., Nestola, F., Bruno, M., Boffa Ballaran, T., Liebske, C., 2008. Thermal expansion along the $\text{NaAlSi}_2\text{O}_6$ - $\text{NaFe}^{3+}\text{Si}_2\text{O}_6$ and $\text{NaAlSi}_2\text{O}_6$ - $\text{CaFe}^{2+}\text{Si}_2\text{O}_6$ solid solutions. *Phys. Chem. Miner.* 35, 241–248.
- Wang, S., Liu, X., Fei, Y., He, Q., Wang, H., 2012. In situ high-temperature powder X-ray diffraction study on the spinel solid solutions $(\text{Mg}_{1-x}\text{Mn}_x)\text{Cr}_2\text{O}_4$. *Phys. Chem. Miner.* 39, 189–198.
- Wang, Z., O'Neill, H.S.C., Lazor, P., Saxena, S.K., 2002. High pressure Raman spectroscopic study of spinel MgCr_2O_4 . *J. Phys. Chem. Solids* 63, 2057–2061.
- Weidner, D.J., Sawamoto, H., Sasaki, S., Kumazawa, M., 1984. Single-crystal elastic properties of the spinel phase of Mg_2SiO_4 . *J. Geophys. Res.* 89, 7852–7860.
- Xiong, Z., Liu, X., Shieh, S.R., Wang, F., Wu, X., Hong, X., Shi, Y., 2015. Equation of state of a synthetic ulvöspinel, $(\text{Fe}_{1.94}\text{Ti}_{0.03})\text{Ti}_{1.00}\text{O}_{0.00}$, at ambient temperature. *Phys. Chem. Miner.* 42, 171–177.
- Yamanaka, T., Takéuchi, Y., 1983. Order-disorder transition in MgAl_2O_4 spinel at high temperatures up to 1700 °C. *Z. für Kristallogr.* 165, 65–78.
- Yamanaka, T., Kyono, A., Nakamoto, Y., Meng, Y., Kharlamova, S., Struzhkin, V.V., Mao, H.-K., 2013. High-pressure phase transitions of $\text{Fe}_{3-x}\text{Ti}_x\text{O}_4$ solid solution up to 60 GPa correlated with electronic spin transition. *Am. Mineral.* 98, 736–744.
- Yong, W., Botis, S., Shieh, S.R., Shi, W., Withers, A.C., 2012. Pressure-induced phase transition study of magnesiochromite (MgCr_2O_4) by Raman spectroscopy and X-ray diffraction. *Phys. Earth Planet. Inter.* 196–197, 75–82.
- Zhang, Y., Liu, X., Xiong, Z., Zhang, Z., 2016. Compressional behavior of MgCr_2O_4 spinel from first-principles simulation. *Sci. China-Earth Sci.* 59, 989–996.